The X-Ray Mirror Telescope and the pn-CCD Detector of CAST

M. Kuster [a], H. Bräuninger [a], J. Englhauser [a], P. Friedrich [a], R. Hartmann [c], R. Kotthaus [b], G. Lutz [b], W. Serber [b], L. Strüder[a], D. Kang [d], J. Franz [d], J. Moralez [e]

[a]Max-Planck-Institut für Extraterrestrische Physik, Giessenbachstr., 85748 Garching, Germany
[b]Max-Planck-Institut für Physik, Föhringer Ring 6, 80805 München, Germany
[c]PNSensor GmbH, Römerstr. 28, 80803 München, Germany
[d]Universität Freiburg – Physikalisches Institut, Herrman-Herder-Str. 3, 79104 Freiburg, Germany
[e]Instituto de Física Nulear y Altas Energías, Universidad de Zaragoza, Zaragoza, Spain

ABSTRACT

The Cern Axion Solar Telescope – CAST – uses a prototype 9 Tesla LHC superconducting dipole magnet to search for a hypothetical pseudoscalar particle, the axion, which was proposed by theory in the 1980s to solve the strong CP problem and which could be a dark matter candidate. In CAST a strong magnetic field is used to convert the solar axions to detectable photons via inverse Primakoff effect. The resulting X-rays are thermally distributed in the energy range of 1–7 keV and can be observed with conventional X-ray detectors. The most sensitive detector system of CAST is a pn-CCD detector originally developed for XMM-Newton combined with a Wolter I type X-ray mirror system. The combination of a focusing X-ray optics and a state of the art pn-CCD detector which combines high quantum efficiency, good spacial and energy resolution, and low background improves the sensitivity of the CAST experiment such that for the first time the axion photon coupling constant can be probed beyond the best astrophysical constraints. In this paper we report on the performance and status of the X-ray telescope and pn-CCD detector of CAST.

Keywords: Solar Axions, Dark Matter, pn-CCD, X-ray Optics, CAST, Low Background

1. INTRODUCTION

The CAST experiment at CERN searches for a novel kind of pseudoscalar particle the axion which was introduced in 1977 as a solution to the strong CP problem.[1] A light axion of a mass in the sub eV range would also be a viable dark matter candidate. For a detailed introduction to the CAST experiment in general and the physics of axion detection we refer the reader to a separate article in this volume.[2] The axion couples to two photons with the strength given by the coupling constant $g_{a\gamma\gamma}$. This coupling would allow the production of axions inside the sun via the Primakoff effect ($\gamma\gamma \rightarrow$ a) resulting in an axion flux proportional to $g^2_{a\gamma\gamma}$. The axion energy spectrum would be thermally distributed peaking at about 3 keV, reflecting the temperature distribution in the core of the sun.[3] In the presence of a transverse magnetic field solar axions can convert to observable X-rays via the inverse Primakoff effect with a probability $P_{a\rightarrow\gamma} \propto g^2_{a\gamma\gamma}(BL)^2$. In CAST we use a 10 m long 9 Tesla superconducting dipole magnet providing a homogeneous transversal magnetic field for this purpose. For given magnet parameters, i.e., the strength of the magnetic field $|\vec{B}|$ and the length L of the magnet the sensitivity of the experiment then solely depends on counting statistics. The expected count rate for the X-ray telescope of CAST in the energy range of 1–7 keV is:

$$\Phi_\gamma \approx 2.59\, g_{10}^4 \,\text{counts}\,\text{day}^{-1} \tag{1}$$

including the effective area of the detector ($g_{10} = g_{a\gamma\gamma} \times 10^{-10}\,\text{GeV}^{-1}$). Thus like in other rare event experiments background reduction is indispensable to increase the sensitivity of the experiment to detect a potential signal. In general, the detector background can be reduced by a proper choice of radiopure detector materials, passive

Send correspondence to M. Kuster: E-mail: kuster@hll.mpg.de, Phone: +49 (0)89 839400 35

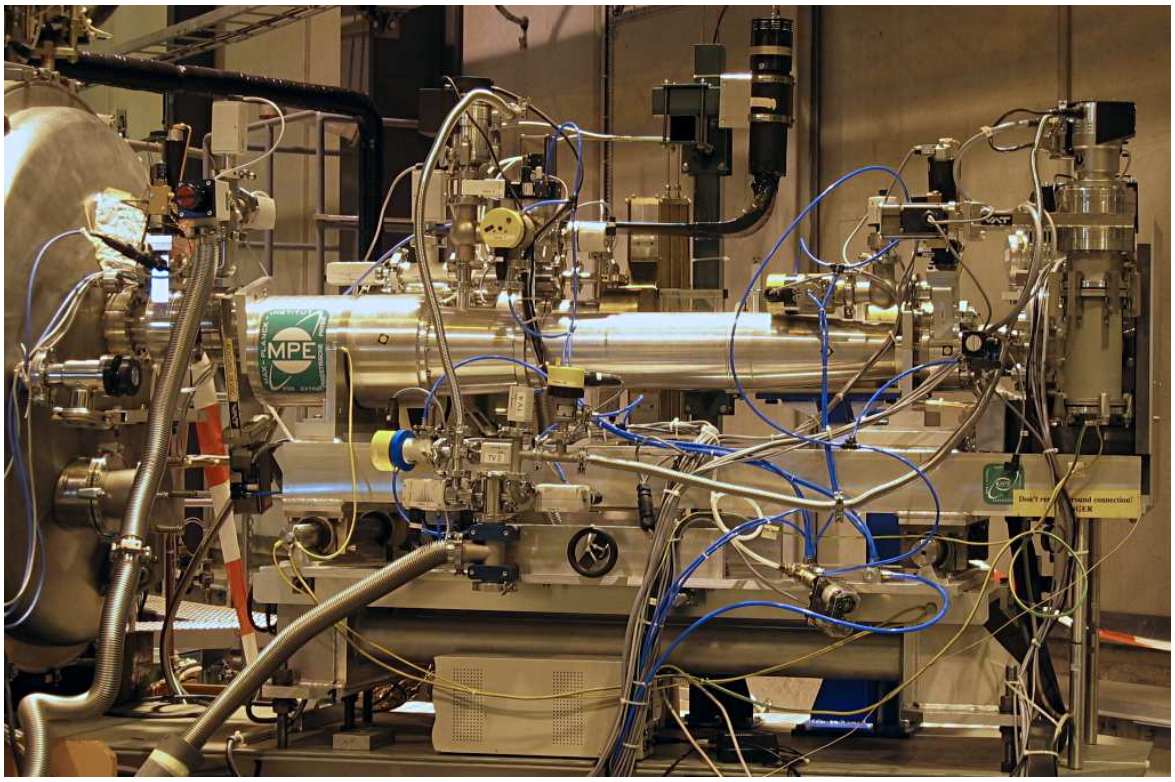

Figure 1. The X-ray telescope and the pn-CCD camera mounted to the superconducting magnet at CERN. The tube visible in the middle of the image is the telescope housing, the magnet bore is to the left, and the CCD detector and it's vacuum system is fixed to the telescope end to the right.

or active shielding of the detector, during data analysis by pattern recognition methods, and by minimizing the active detector volume. In CAST the last method is exploited by focusing the expected signal to a small area on the detector. In this paper we report on the performance and design of the X-ray telescope and the pn-CCD detector and its shielding concept.

2. THE X-RAY TELESCOPE

The Wolter I type X-ray mirror telescope of CAST is a prototype of the German X-ray satellite mission ABRIXAS which after a successful launch unfortunately failed in 1999.[4–6] The telescope is assembled to one of the two magnet bores on the side of the magnet which is facing the rising sun as shown in Fig. 1. It consists of a combination of 27 nested and gold coated parabolic and hyperbolic mirror shells with a focal length of 1600 mm. The maximum diameter of the outermost mirror shell is 163 mm while the smallest shell has a diameter of 76 mm, only.[7] A spider like structure (see Fig. 2) supports the individual mirror shells on their front side and divides the aperture of the telescope into six sectors. Since the bore of the CAST magnet has a diameter of 43 mm, only a fraction of the full aperture of the telescope is used in CAST. For this reason, the telescope is fixed to the magnet non-centrically such that only one of the six mirror sectors is illuminated by the nearly parallel X-ray beam emerging from axion to photon conversion inside the magnet. The telescope is operated under vacuum conditions at a pressure below 10^{-5} mbar to prevent contamination and adsorption on the mirror reflective surface which would result in a degradation of the efficiency of the telescope system.

2.1. Effective Area and Point Spread Function

The overall performance of an X-ray telescope for a given focal length mainly depends on two parameters, the effective area and the spatial resolution, given by the point spread function (PSF). The effective area in

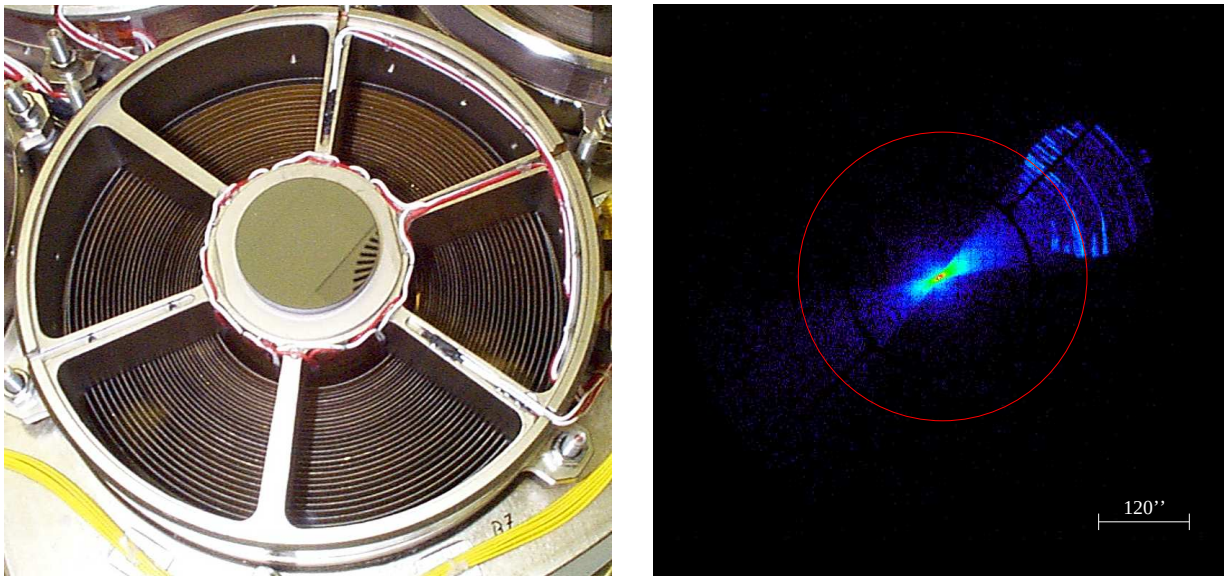

Figure 2. Left: Front view of the mirror system. The individual mirror shells and the supporting spoke structure are shown. One of the six sectors is illuminated by the magnet bore. Right: Logarithmic intensity image of the point spread function of one mirror sector measured with the PSPC detector at the PANTER test facility. For comparison, the red circle indicates the expected spot size of a solar axion signal. Due to the fact that the X-ray source is at a finite distance ($d \approx 100\,\mathrm{m}$), photons reflected only by one of the parabolic or hyperbolic shaped surfaces are apparent in the image (single reflections).

general is a function of the off-axis angle, the micro roughness of the mirror surfaces, and the photon energy. It decreases with increasing micro roughness, photon incidence angles (lower reflectivity), and due to geometric effects (vignetting). To determine the PSF and the effective area, we made extensive calibration measurements of all six mirror sectors at the PANTER test facility in Munich using monoenergetic X-rays of different energies. The resulting on-axis angular resolution of the telescope is 34 arcsec (HEW) at 1.5 keV and 43 arcsec (HEW) at 8.0 keV which is almost a factor of 10 better than the expected size of the "axion image" of the sun (see Fig. 2).

In addition, the effective area of the telescope depending on energy was measured for each individual sector of the telescope. The results are summarized in Tab. 1. The telescope sector 4 with the best effective area was chosen for CAST. The on-axis effective area of this sector is shown in the left part of Fig. 3 for a telescope aperture with a diameter of 48 mm, which was the setup of the calibration measurements at the PANTER test facility. In order to transfer these results to an aperture of 42 mm, which is the diameter of the CAST magnet bore, we made ray-tracing simulations for both diameters, 48 mm and 42 mm. These simulations include the mirror system with the mirror support structure and the magnet tube geometry assuming a perfectly straight

Table 1. Effective area of the individual mirror sectors as measured at the PANTER test facility.

Sector	Effective area [cm^2]			
	0.93 keV	1.49 keV	4.5 keV	8.04 keV
1	13.5	13.4	8.2	3.9
2	13.5	13.4	8.2	3.8
3	8.9	13.6	8.3	3.9
4	13.9	13.9	8.4	4.0
5	12.6	12.8	7.9	3.4
6	13.1	13.4	8.5	4.0

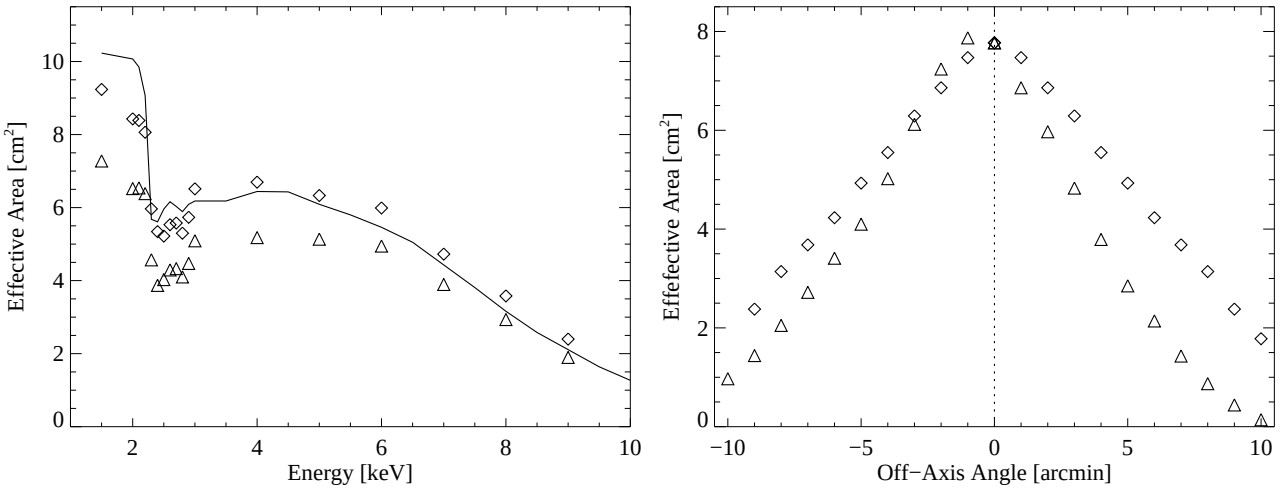

Figure 3. Left: On-axis effective area of the X-ray telescope. Three different cases are shown, the effective area measured at PANTER with an aperture of 48 mm (diamonds), simulated effective area for the same aperture (solid line), and the expected effective area for a telescope aperture of 42 mm (triangles). Right: Influence of the vignetting effect on the effective area of the X-ray telescope for photons with an energy of 1.5 keV, for radial (triangles) and tangential off-axis angles (diamonds).

beam pipe. As a result we get the energy dependant on-axis effective area and the vignetting function depending on energy and off-axis angle. The simulated on-axis effective area is shown in Fig. 3 as a solid line for a telescope aperture with a diameter of 48 mm. The effective area for a 42 mm aperture is shown as triangles, which are the results of of the PANTER measurements scaled with the ratio of the simulated effective areas for a 48 mm and 42 mm aperture. The off-axis behavior is shown in the right part of Fig. 3 for off-axis angles in radial and tangential direction. The asymmetric experimental setup with one of six sectors being illuminated, causes a difference between the tangential and the radial off-axis behavior. This results in a slightly asymmetric point spread function and an asymmetry in the vignetting due to the magnet beam pipe and the telescope structure. The asymmetry of the PSF is apparent from the differently pronounced side-lobes of the PSF in Fig. 2 (note that this effect is not of importance for CAST since the expected size of the spot of a solar axion signal is much larger). To demonstrate the influence of the magnet beam pipe geometry on the efficiency of the telescope, the contribution of the magnet and of the telescope geometry to the total vignetting losses are shown in Fig. 4. It is apparent that for a slight misalignment, the telescope off-axis effective area together with additional vignetting from the magnet beam pipe reduces the sensitivity of the instrument noticeable (for deviations > 2 arcmin the efficiency reduces by more than 10%).

3. THE PN-CCD DETECTOR

X-rays originating in axion to photon conversions inside the magnet would be focused by the telescope system onto the pn-CCD focal plane detector producing an "axion image" of the sun. A detailed summary on the performance and characteristics of the pn-CCD detector in general can be found in Ref.[8] and references therein. In the following sections we will concentrate on the description of the design of the detector system for CAST and the detector parameters that are relevant for the sensitivity of the experiment.

3.1. Detector Design and Characteristics

The pn-CCD detector for CAST is a prototype of the 280 μm thick, fully depleted EPIC pn-CCD on-board of ESA's XMM-Newton mission which was developed at our institute.[8] The CCD chip has a sensitive area of 2.88 cm^2 divided into 200×64 pixels. Each pixel has a size of $150 \times 150\,\mu$m which corresponds to an angular resolution of 19.08×19.08 arcsec^2/pixel for a focal length of 1600 mm. Thus the CCD is larger than the expected image of the innermost part of the Sun ($0.2R_\odot$) where axions are produced most efficiently. The apparent diameter of the "axion image" of the sun is 19 pixels = 2.83 mm. This allows to measure background and a

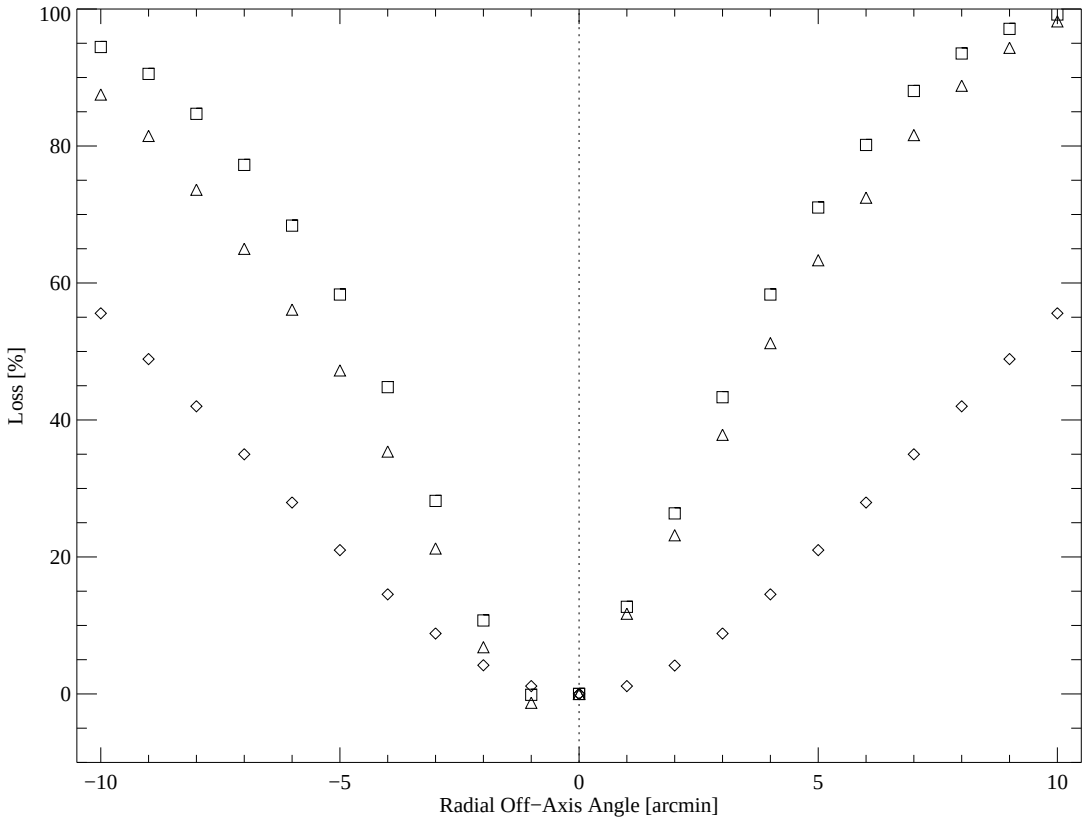

Figure 4. Loss in efficiency due to geometric effects (vignetting) for photons with an energy of 1.5 keV. Three different cases are shown: vignetting due to the magnet bore geometry assuming a realistic extended axions source (diamonds), vignetting due to the telescope geometry (triangles), and the total vignetting effect (rectangles).

potential axion signal at the same time, which reduces systematic effects due to background variations to a minimum. The operating temperature of the CCD is −130 C and is kept stable over time with a Stirling cooler system. The thermal coupling between the cooling system and the CCD is provided by flexible copper leads connecting the cold finger of the Stirling cooler with the cooling mask of the CCD chip (see Fig. 5). The most important parameters of the detector are summarized in the table of Fig. 5. One of the major advantages of this type of solid state X-ray detector is the high quantum efficiency close to unity due to its very thin (20 nm) and uniform radiation entrance window on the backside of the chip.[8] This allows to operate the detector in vacuum without any additional window. Since the CCD is operated continuously and is sensitive to photons all the time, the detector has no physical dead time.

3.2. Detector Background

The main contributions to the background of the pn-CCD detector is background induced by cosmic rays, gamma rays, and radioactive impurities in the magnet and the detector materials. To reduce the external gamma ray background we implemented a combination of a copper and lead shield inside the evacuated housing of the pn-CCD detector (see Fig. 7). Starting with the cooling mask which is the component closest to the detector, a copper shield follows which consist of a 10 − 40 mm thick copper box made of oxygen free and low activity copper. The copper box covers the full CCD detector and has a 40 mm aperture towards the telescope (see Fig. 7). The copper box is surrounded by 22 mm lead encapsulated in a 2 mm thick layer of copper which is a precaution to prevent vacuum contamination. To reduce the activity of ^{210}Pb, which is the most significant contamination of ordinary lead, we used old ballast lead of a sunken galleon stored underground for longer than several half-life

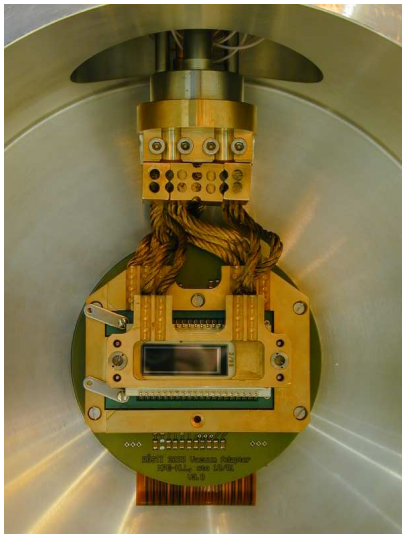

Characteristics of the pn-CCD detector.

Geometry	200×64 Pixels
Pixel size	$150 \times 150\,\mu$m
Depletion Depth	$280\,\mu$m
Energy Resolution (FWHM)	160 eV@ 6 keV
Quantum Efficiency $(1-7\,\text{keV})$	$> 95\,\%$
Operating Temperature	$-130°$ C
Cycle Time t_{int}	71.775 ms
Readout Time t_{read}	6.06 ms

Figure 5. The pn-CCD chip (black part in the center) with the gold plated cooling mask which is connected to a cold finger of a Stirling cooler device.

times of ^{210}Pb ($t_{1/2} = 22$ years). A second lead shield of the same material outside the detector chamber protects the system against environmental backgrounds.

Based on the good spatial resolution of the detector the background can further be reduced. Using pattern recognition techniques it is possible to efficiently identify minimum ionizing particles in the data and remove such events. The rejection of cosmic ray related events does not lead to efficiency losses in the photon energy range of interest for the axion search. The resulting background spectrum of data taken in 2003 after having applied all corrections is shown in Fig. 6. The remaining mean background corresponds to a mean differential flux of $(7.5 \pm 0.2) \times 10^{-5}$ counts cm^{-2} sec^{-1} keV^{-1} in the axion sensitive energy range $(1-7\,\text{keV})$ and is extremely low for an experiment above surface. Above 7 keV the background spectrum is dominated by fluorescent line emission (Cu-Kα and Cu-Kβ lines) originating in the cooling mask close to the detector chip. A weak blend of the Au-L lines can be identified between 9 and 10 keV which arise from fluorescence of the gold plated surface of the cooling mask. Below 7 keV the background is dominated by a flat Compton continuum of predominantly backscattered photons. A weak Cu escape line feature appears close to 6.2 keV.

In the actual shielding concept of the pn-CCD detector, radioactive impurities in the materials close to the CCD chip are not yet taken into account. Nevertheless, for further background suppression in future approaches of the experiment by proper selection of the detector materials, we measured all detector components close to the CCD chip and the pn-CCD chip itself in the low background laboratory of the University of Saragossa. A summary of the activities for the most dominant contaminants of the detector components are given in Tab. 2. Since silicon is one of the cleanest materials available we did not expect a major contribution to the background from the CCD chip itself. According to the measurement the contamination of the Si is negligible and below the sensitivity of the measurement. The ceramics substrate (carrier of the CCD) and the electronic circuit board (located behind the CCD) contribute most to the background due to natural radioactivity. Both are slightly contaminated by ^{238}U, ^{235}U, and ^{40}K. Since the cooling mask almost fully covers the ceramic substrate and the zero force socket, it shields the active region of the CCD against gammas emitted by both components. Simulations using the GEANT4 Monte Carlo simulation package, that will allow us to estimate the influence of natural radioactivity on the overall pn-CCD background are in progress.

4. CONCLUSIONS AND PROSPECTS

The mirror telescope of CAST is in operation since summer 2003 and is taking data in routine operation. The combination of a focusing optics and a detector with high spatial resolution can improve the sensitivity in rare event experiments as in CAST. In the case of CAST we expect an improvement of the signal to background

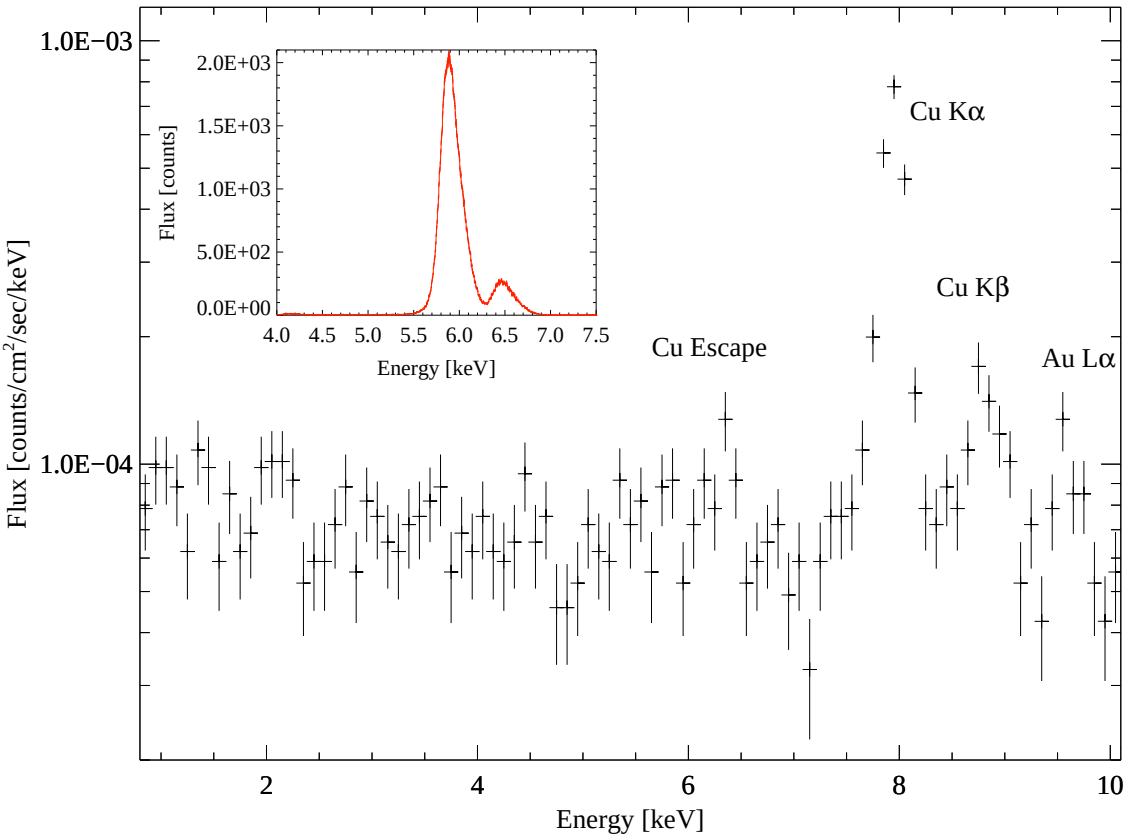

Figure 6. A typical background spectrum observed with the pn-CCD detector. The most prominent emission lines apparent are the fluorescent lines of Cu at $\approx 8\,\mathrm{keV}$ and 8.9 keV and Au-Lα at $\approx 9.6\,\mathrm{keV}$. Inlayed plot: A calibration spectrum of an ^{55}Fe source demonstrating the energy resolution of the detector (FWHM $\approx 160\,\mathrm{eV}$).

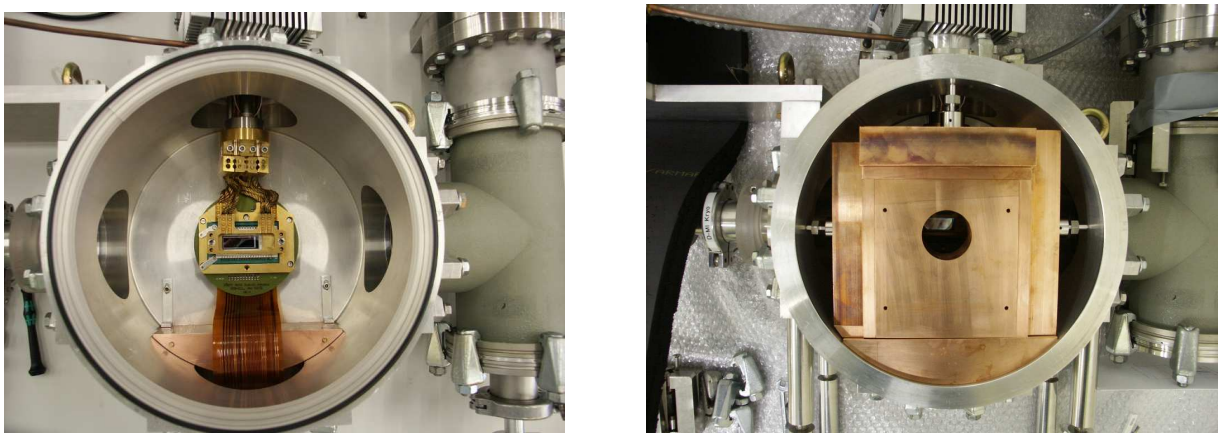

Figure 7. Left image: Front view of the CAST pn-CCD detector housing showing the pn-CCD chip and vacuum components on the right side. Right image: The pn-CCD detector with inner shielding components. The shield consists from the outer to the inner parts: a 2 cm thick layer of oxygen free, low activity copper, and a layer of 2.2 cm thick layer of low activity, ancient lead encapsulated in copper. An additional 2.5 cm lead shield is installed outside the vacuum housing of the detector.

Table 2. Activity of the detector materials as measured in the low background laboratory of the University of Saragossa. Activities are given in units of mBq/g.

Detector component	^{238}U	^{235}U	^{232}Th	^{40}K	^{60}Co
Circuit Board	17.2 ± 0.8	0.9 ± 0.1	15.6 ± 1.3	10.6 ± 1.7	
Ceramic Substrate	20 ± 4		4.3 ± 0.7	20 ± 4	
Cooling Mask				2.9 ± 0.1	< 0.01
CCD Chip				< 4	< 0.2

ratio by a factor of ≈ 200. In terms of the axion coupling constant $g_{a\gamma\gamma}$ this is equivalent to an improvement of the upper limit by a factor of 1.9 compared to a non-focusing detector. We expect a further improvement in background by $\approx 20\,\%$ due to a better cosmic ray rejection algorithm which takes into account cosmic ray induced X-rays as well. This algorithm rejects the whole image of one read out cycle, instead of rejecting only the pixels with a signal due to cosmic ray interaction. We want to point out that this technique can reject cosmic ray induced X-rays only for the case that both, the X-ray photon and the cosmic ray give a signal in the detector. For this reason an active anticoincidence close to the CCD would improve the background rejection. Further background reduction could be achieved by a rebuilding of the detector components from materials selected for radiopurity and with a graded-Z shield close to the CCD which acts as an absorber for low energy photons ($E < 7\,\mathrm{keV}$).

ACKNOWLEDGMENTS

This work is supported by the Bundesministerium für Bildung und Forschung (BMBF) under the grant number 05 CC2EEA/9.

REFERENCES

1. R. D. Peccei and H. R. Quinn, "CP conservation in the presence of pseudoparticles," *Phys. Rev. Lett.* **38**, pp. 1440–1443, June 1977.
2. M. Kuster, "The CERN solar axion telescope (CAST): A status report," 2004. this volume.
3. K. van Bibber, P. M. McIntyre, D. E. Morris, and G. G. Raffelt, "Design for a practical laboratory detector for solar axions," *Phys. Rev. D* **39**, pp. 2089–2099, Apr. 1989.
4. J. Altmann, W. J. Egle, U. Bingel, W. Hafner, B. Gaenswein, H. Schwarz, and A. Neugschwender, "Mirror system for the German X-ray satellite ABRIXAS: I. Flight mirror fabrication, integration, and testing," in *X-Ray Optics, Instruments, and Missions II*, R. B. Hoover and A. B. Walker, eds., *Proceedings of SPIE*, pp. 350–358, SPIE, (Bellingham, WA), Nov. 1998.
5. W. J. Egle, J. Altmann, P. Kaufmann, H. Muenker, G. Derst, H. Schwarz, and A. Neugschwender, "Mirror system for the German X-ray satellite ABRIXAS: II. Design and mirror development," in Hoover and Walker,[10] p. 359.
6. G. Hasinger, J. Trumper, and R. Staubert, "Abrixas," in *IAU Symp. 188: The Hot Universe*, p. 83, 1998.
7. P. Friedrich, H. W. Braeuninger, W. Burkert, T. Doehring, R. Egger, G. Hasinger, A. Oppitz, P. Predehl, and J. Truemper, "X-ray tests and calibrations of the ABRIXAS mirror systems," in Hoover and Walker,[10] p. 369.
8. L. Strüder, U. Briel, K. Dennerl, R. Hartmann, E. Kendziorra, N. Meidinger, E. Pfeffermann, C. Reppin, B. Aschenbach, W. Bornemann, H. Bräuninger, W. Burkert, M. Elender, M. Freyberg, F. Haberl, G. Hartner, F. Heuschmann, H. Hippmann, E. Kastelic, S. Kemmer, G. Kettenring, W. Kink, N. Krause, S. Müller, A. Oppitz, W. Pietsch, M. Popp, P. Predehl, A. Read, K. H. Stephan, D. Stötter, J. Trümper, P. Holl, J. Kemmer, H. Soltau, R. Stötter, U. Weber, U. Weichert, C. von Zanthier, D. Carathanassis, G. Lutz, R. H. Richter, P. Solc, H. Böttcher, M. Kuster, R. Staubert, A. Abbey, A. Holland, M. Turner, M. Balasini, G. F. Bignami, N. La Palombara, G. Villa, W. Buttler, F. Gianini, R. Lainé, D. Lumb, and P. Dhez, "The European Photon Imaging Camera on XMM-Newton: The pn-ccd camera," *Astron. Astrophys.* **365**, pp. L18–L26, Jan. 2001.

9. G. Lutz, H. Bräuninger, J. Englhauser, R. Hartmann, D. Kang, R. Kotthaus, M. Kuster, W. Serber, and L. Strüder, "An application of space technology to the terrestrial search for axions: The X-ray mirror telescope at CAST," *Nuclear Instruments and Methods in Physics Research A* **518**, pp. 201–206, Feb. 2004.
10. R. B. Hoover and A. B. Walker, eds., *X-Ray Optics, Instruments, and Missions*, *Proceedings of SPIE*(3444), (Bellingham, WA), SPIE, 1998.